iScience

CellPress

Article

Chemical-Chemical Combinations Map Uncharted Interactions in *Escherichia coli* under Nutrient Stress

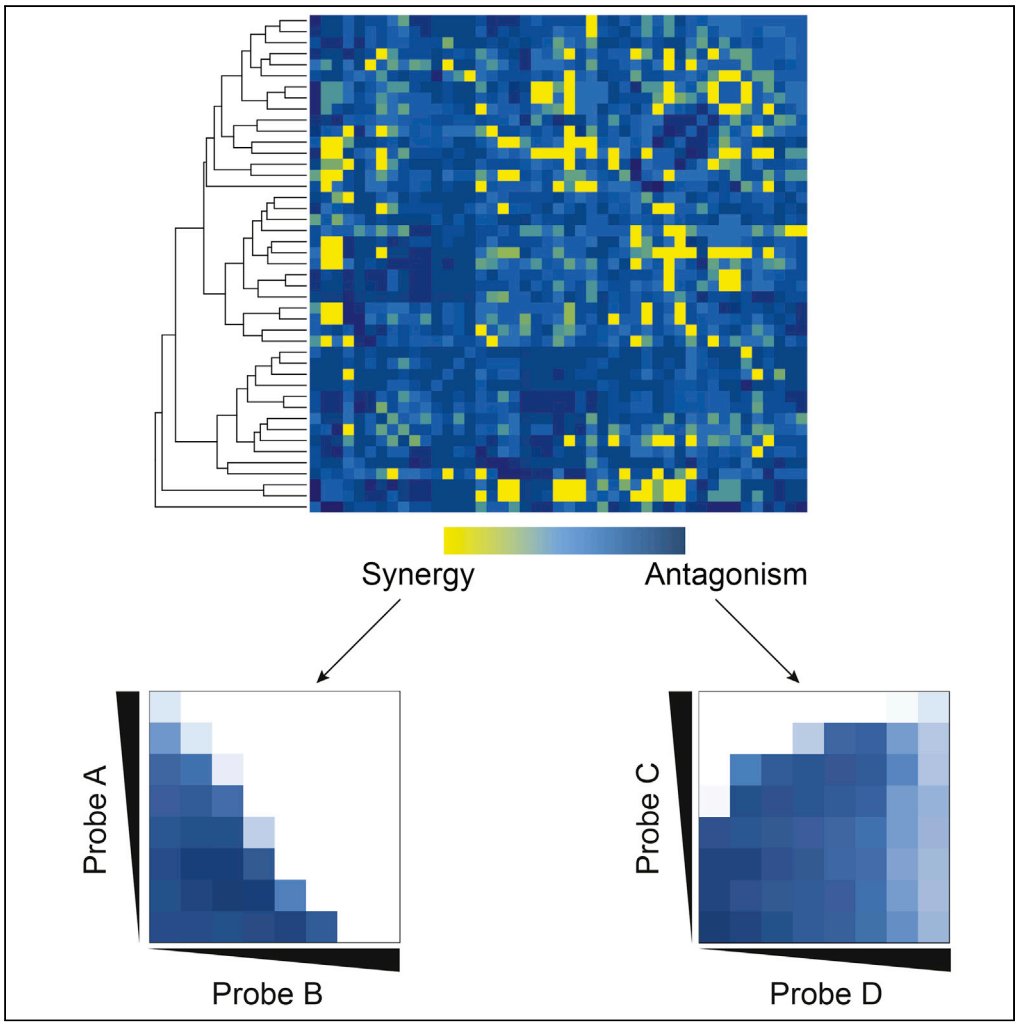

Sara S. El Zahed, Eric D. Brown

ebrown@mcmaster.ca

HIGHLIGHTS

Chemical probes map a complex interaction network in *E. coli* under nutrient stress

A total of 990 unique chemical combinations reveal a dense network of 186 interactions

New connections between housekeeping functions and those in nutrient stress

El Zahed & Brown, iScience *2*, 168–181
April 27, 2018
https://doi.org/10.1016/j.isci.2018.03.018

iScience

CellPress

Article

Chemical-Chemical Combinations Map Uncharted Interactions in *Escherichia coli* under Nutrient Stress

Sara S. El Zahed[1,2] and Eric D. Brown[1,2,3,*]

SUMMARY

Of the ~4,400 genes that constitute *Escherichia coli*'s genome, ~300 genes are indispensable for its growth in nutrient-rich conditions. These encode housekeeping functions, including cell wall, DNA, RNA, and protein syntheses. Under conditions in which nutrients are limited to a carbon source, nitrogen source, essential phosphates, and salts, more than 100 additional genes become essential. These largely code for the synthesis of amino acids, vitamins, and nucleobases. Although much is known about this collection of ~400 genes, their interactions under nutrient stress are uncharted. Using a chemical biology approach, we focused on 45 chemical probes targeting encoded proteins in this collection and mapped their interactions under nutrient-limited conditions. Encompassing 990 unique pairwise chemical combinations, we revealed a highly connected network of 186 interactions, of which 81 were synergistic and 105 were antagonistic. The network revealed signature interactions for each probe and highlighted new connectivity between housekeeping functions and those essential in nutrient stress.

INTRODUCTION

Systematic analyses of genome-scale gene deletion collections have characterized the basic housekeeping functions for bacterial survival. Such studies in the model bacterium *Escherichia coli*, for example, have shown that 303 genes have an essential phenotype for growth in nutrient-rich conditions, whereas the balance, approximately 4,000 genes, are dispensable (Baba et al., 2006). In nutrient-limited conditions, wherein *E. coli* is grown in a medium containing glucose and ammonium chloride (carbon and nitrogen sources, respectively) as well as essential phosphates and salts, a total of 422 genes have an indispensable phenotype (Baba et al., 2006; Joyce et al., 2006). This additional set of 119 genes largely encodes proteins required for the synthesis of amino acids, vitamins, nucleobases, and other cofactors. Although much is known about these housekeeping and nutrient stress functions, our understanding comes from studies that are mainly reductionist in nature, derived from one-gene-at-a-time experiments examining cell physiology or from biochemical studies of the encoded protein (Baba et al., 2006; Joyce et al., 2006; Nichols et al., 2011). Lacking, however, is an understanding of the interaction of these functions with one another as well as with the greater cell system.

We recently studied the interaction of nutrient stress genes with the dispensable gene set under nutrient-rich conditions using a synthetic lethality approach (Côté et al., 2016). Some 82 nutrient stress genes (of 119) were crossed with nearly 4,000 single gene deletion mutants to identify synthetic sick or lethal interactions. With a total of 1,881 such interactions, this study revealed a large number and density of synthetic lethal (or sick) gene combinations for the query gene set. This work revealed signature interactions between nutrient acquisition and biosynthesis as well as pathway redundancies and the presence, in this network, of a surprising number of genes of unknown function. Of course, this gene-gene interaction dataset was collected in nutrient-rich conditions, in which nutrient stress genes are dispensable. Accordingly, the dataset lacks any insight into the genetic network under nutrient-limited conditions, wherein nutrient stress genes have an essential phenotype. Indeed, although genetic mutation is the dominant approach to studying genetic networks, genes with indispensable phenotypes have largely resisted characterization with network mapping tools. Only in the model yeast, *Saccharomyces cerevisiae*, in which temperature-sensitive alleles have been created in hundreds of essential genes, has synthetic lethality been used to map the interaction network of genes with essential phenotypes (Costanzo et al., 2016; Li et al., 2011). This effort showed that essential genes had many more interactions on average than dispensable genes and established these functions as hubs in the global genetic network of *S. cerevisiae*.

[1]Department of Biochemistry and Biomedical Sciences, McMaster University, Hamilton, ON L8N 3Z5, Canada

[2]Michael G. DeGroote Institute of Infectious Disease Research, McMaster University, Hamilton, ON L8N 3Z5, Canada

[3]Lead Contact

*Correspondence: ebrown@mcmaster.ca

https://doi.org/10.1016/j.isci.2018.03.018

Category	Interactions		
	Synergy	Antagonism	Total
HK probes[a]	18	39	57
NS probes[b]	22	19	41
HK probes and NS probes[c]	41	47	88
Total	81	105	186

Table 1. Categories of Interactions among Chemical Probes of *E. coli* under Nutrient Stress

[a]HK probes, housekeeping-function probes, refer to 27/45 compounds that target housekeeping functions (Data S1). Interactions belonging to the HK probes category involve 49 antibiotic-antibiotic and 8 lamotrigine-antibiotic combinations.
[b]NS probes, nutrient synthesis probes, refer to 18/45 compounds that target nutrient synthesis functions (Data S1). Interactions belonging to the NS probes category involve combinations between these 18 nutrient synthesis probes.
[c]Interactions belonging to the HK probes and NS probes category involve interactions between a housekeeping-function probe and a nutrient synthesis probe.

In the work described here, we have taken a chemical biology approach (Parsons et al., 2004) to study the interaction network of housekeeping and nutrient stress functions in *E. coli* under nutrient-limited conditions, in which all of the associated genes are essential for growth. We targeted these functions with 45 chemical probes using a matrix of 990 pairwise chemical combinations. The compounds were systematically combined in 64-dose checkerboard matrices, referred to here as checkerboard assays, and assessed for the interaction phenotype of growth inhibition: synergy, antagonism, or indifference (no interaction). When growth inhibition that results from combining two compounds is simply the sum of effects of individual compounds, this is referred to as indifference. In contrast, synergy and antagonism describe phenotypic interactions that lead to more or less growth inhibition, respectively, than predicted by the sum of the individual effects of the two compounds. Some 81 synergistic and 105 antagonistic interactions were recorded, suggesting that essential functions represent a highly connected network in bacteria. We further investigated some especially potent and paradoxical interactions between biotin and fatty acid synthesis, amino acid biosynthesis and ribosome assembly, as well as purine synthesis and protein translation inhibition. In all, the work highlighted a high density of interactions among essential functions as well as unique connectivity between nutrient biosynthesis and housekeeping functions in bacteria.

RESULTS

Chemical-Chemical Interaction Matrix

Some 45 compounds, known to probe bacterial functions in nutrient synthesis and housekeeping functions, were selected to generate a systematic analysis of chemical-chemical combinations to determine the nature of each interaction, i.e., synergistic, antagonistic, or indifferent (no interaction). The 45 compounds included 18 nutrient synthesis probes with growth inhibitory activities restricted to nutrient-limited conditions and 27 housekeeping-function probes that included antibiotics that target cell wall, protein synthesis, or DNA replication and lamotrigine, a compound that was recently identified to be an inhibitor of bacterial ribosome biogenesis (Stokes et al., 2014). A list of the probes and their targets is provided in supplementary data (Data S1). We systematically characterized the interaction of these 45 compounds with one another using checkerboard assays that analyzed the concentration dependence of the activity of pairs of compounds. The phenotype tested for was the inhibition of *E. coli* growth in the nutrient-limited medium, M9 minimal, which consisted of only glucose as the carbon source, ammonium chloride as the nitrogen source, essential phosphates, and salts. Binary combination space for n compounds is defined by the formula n*(n-1)/2 (Keith et al., 2005). Thus, 990 pairs of compounds were tested using a total of 63,360 individual data points. An analysis of the checkerboard data revealed the nature of these pairwise interactions. The fractional inhibitory concentration index (FICI) was calculated for each checkerboard assay (Transparent Methods). FICI is the sum of the fractional inhibitory concentration (FIC) of each tested compound, where the FIC for each tested compound is the ratio of its minimal inhibitory concentration (MIC) in combination divided by its MIC when used on its own (Krogstad et al., 1986). Combinations with an FICI less than or equal to 0.5 were deemed synergistic, whereas those with an FICI greater than 2 were antagonistic and those with an FICI greater than 0.5 and less than or equal to 2 were indifferent (Krogstad et al., 1986). Of the 990 unique pairwise chemical combinations, 81 were synergistic and 105 were antagonistic, resulting in 186 interactions (Table 1 and Figure S1). Thus, on average, each compound

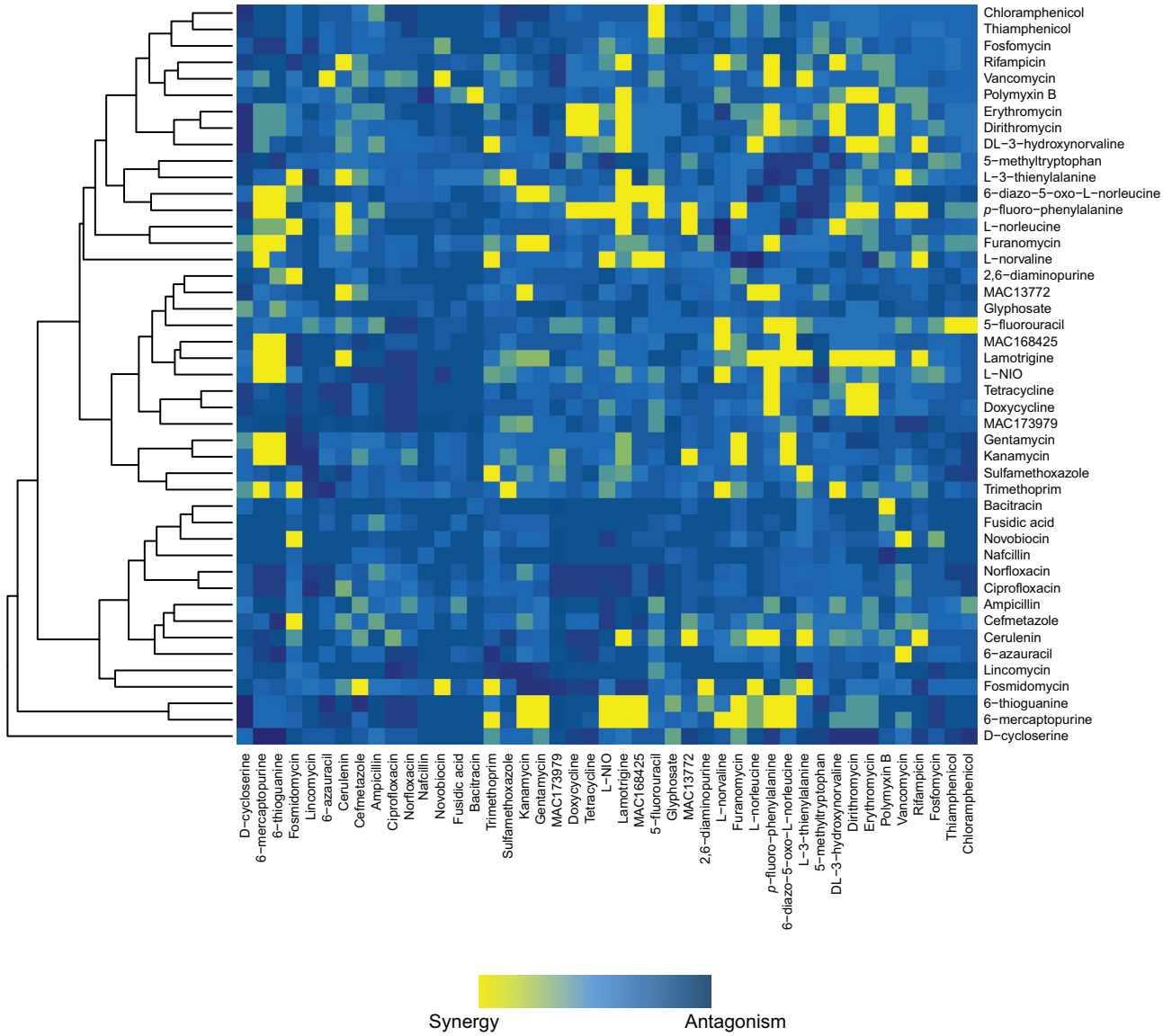

Figure 1. Chemical-Chemical Interaction Matrix under Nutrient-Limited Conditions

A heatmap of systematic chemical-chemical combinations of 45 compounds (990 unique combinations) were assessed for their growth inhibitory effects on *E. coli* BW25113 grown in M9 minimal medium. Interactions in the heatmap are color coded for the nature of the interaction as described by the fractional inhibitory concentration index (FICI) of a systematic dose response analysis of the two compounds, referred to here as checkerboard analysis and described in the Results and Transparent Methods sections. Of the 990 combinations, 81 were synergistic (yellow) and 105 were antagonistic (dark blue). Hierarchical clustering was performed based on the combination profile of each compound. See also Figures S1 and S2 and Data S1 and S2.

had approximately 4 interactions (186/45) with other bioactive compounds. Furthermore, this dataset defined a unique interaction profile for each of the 45 compounds. Figure 1 presents a heatmap of the entire interaction map, hierarchically clustered according to the interaction profiles of each chemical compound. All FICI values for the latter are provided in supplemental data (Data S2).

A large fraction, some 19% (186/990) of these probe combinations, showed interactions suggesting that targeted functions represent a highly connected network in bacteria. While these compounds were selected to probe a diverse array of bacterial physiology, we included some redundancy in our selection of housekeeping-function probes, for example, two phenicols (chloramphenicol and thiamphenicol), two macrolides (erythromycin and dirithromycin), two fluoroquinolones (norfloxacin and ciprofloxacin), and

two tetracyclines (tetracycline and doxycycline). Interestingly, we noted subtle differences among the interaction profiles of closely related probes; however, even if we account for some redundancy by estimating the set of non-redundant probes to be 35 compounds, for example, we still see interactions for about 20% of our combinations. In all, this analysis represents the first comprehensive study to explore the interaction of chemical probes, targeting housekeeping functions and nutrient synthesis, when cells are grown under nutrient-limited conditions. Table 1 summarizes and categorizes the 186 interactions seen.

A total of 57 interactions occurred among the 27 probes of housekeeping functions. Previous antibiotic combination studies have charted interactions between the different classes of antibiotics (Ocampo et al., 2014; Wambaugh et al., 2017; Yeh et al., 2006), which were largely confirmed by our dataset of antibiotic combinations. An interesting pair of interactions identified in this study was the potentiation of the narrow-spectrum Gram-positive antibiotic novobiocin (Cozzarelli, 1977) against *E. coli* by two cell wall-active antibiotics, vancomycin and fosmidomycin (Figure S2). The latter interaction has not been reported by previous antibiotic combination studies. These interactions were curious; however, we have focused herein on new chemical-chemical interactions of relevance to the study of nutrient stress in bacteria.

Interestingly, of the total 186 charted interactions, 129 involved nutrient synthesis probes. Specifically, 88 interactions were between one of the 18 nutrient synthesis probes and the remaining 27 probes targeting housekeeping functions and 41 interactions involved combinations of nutrient synthesis probes. Below, we highlight some illustrative and paradoxical interactions in these categories in addition to presenting a deeper analysis of the interactions seen with probes of biotin, S-adenosylmethionine (SAM), and purine synthesis.

Hierarchical Clustering of Chemical-Chemical Interactions

Hierarchical clustering revealed that probes mapped largely based on the chemical class of each compound. This was an encouraging result from the perspective of data quality because compounds of similar structure naturally share the same mechanism of action (MOA) and thus similar chemical-chemical interaction profiles. For example, norfloxacin and ciprofloxacin belong to the fluoroquinolone antibiotic class and inhibit DNA synthesis by targeting DNA gyrase and topoisomerase IV (Drlica et al., 2008). They show a unique fingerprint of antagonistic interactions with the tetracyclines, chloramphenicol, and the thiopurine analogs (6-thioguanine and 6-mercaptopurine) (Figure 2A). The macrolides, erythromycin and dirithromycin, inhibit protein synthesis by targeting the 50S ribosome (Menninger and Otto, 1982). They have a similar profile of interactions, including antagonistic interactions with gentamycin and D-cycloserine and synergistic interactions with the tetracyclines, polymyxin B, DL-3-hydroxynorvaline, lamotrigine, and *p*-fluoro-phenylalanine (Figure 2B). Similarly, analogs of nutrient synthesis probes, such as the thiopurine analogs 6-thioguanine and 6-mercaptopurine, which incorporate into DNA or RNA and inhibit purine synthesis (Nelson et al., 1975), had similar interaction profiles (Figure 2C). Interactions unique to these compounds include 6-mercaptopurine's synergistic interactions with L-norvaline and trimethoprim as well as 6-thiogunaine's antagonistic interaction with cefmetazole. These observations emphasize the concept that compounds with similar MOA exhibit similar interactions when used in combination with other probes of biology.

Occasionally, interaction profiles clustered together due to a synergistic interaction between the two compounds. For instance, the interaction profiles of sulfamethoxazole and trimethoprim cluster with one another, yet they only share one common antagonistic interaction with lincomycin (Figure 1). Similarly, DL-3-hydroxynorvaline, a threonine analog (Minajigi et al., 2011), synergizes with the macrolides, erythromycin and dirithromycin, and clusters with these compounds; however, each compound's profile is largely distinct. Nonetheless, compounds with a shared MOA largely exhibit substantially similar chemical interaction profiles (Figure 1). Accordingly, the chemical-chemical interaction matrix has strong potential as a tool to elucidate the MOA of new antibacterial compounds, tested under nutrient-limited conditions.

Consistent with the goals of understanding the network that underpins nutrient stress in bacteria, we have focused herein on the interactions that impinge on targets associated with nutrient synthesis. Of the 129 interactions in this category, we prioritized three synergistic interactions that help to elaborate the nutrient stress network in vitamin, amino acid, and nucleobase biosynthesis. Accordingly, we elaborate here on the synergistic interactions that we characterized between MAC13772 and cerulenin, L-norleucine and

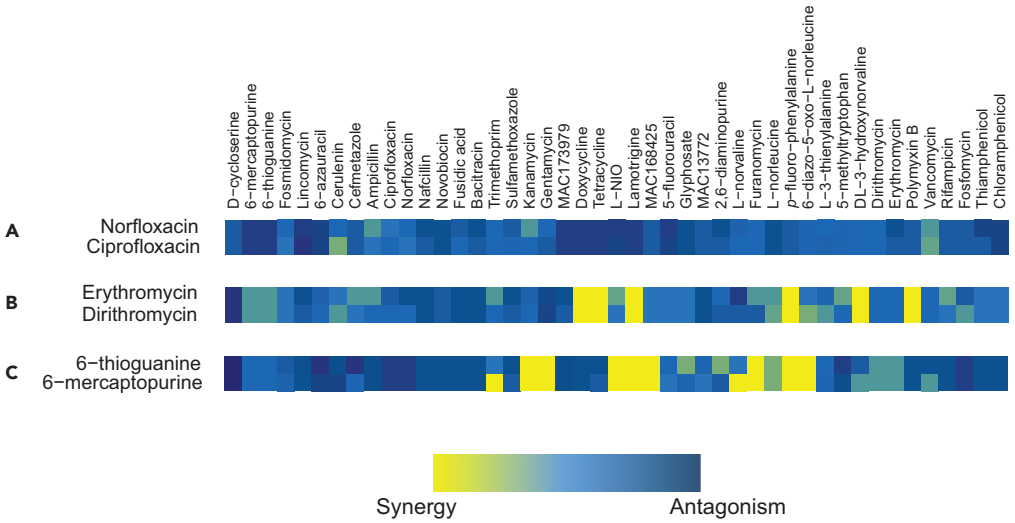

Figure 2. Interaction Profiles Cluster Based on Chemical Class and Mechanism

Compounds belonging to the same chemical class resulted in similar signature interactions with the listed 45 compounds.

(A) The two fluoroquinolone antibiotics, norfloxacin and ciprofloxacin, antagonized the tetracyclines, chloramphenicol, and the thiopurine analogs.

(B) Similarly, the macrolide class of antibiotics, specifically erythromycin and dirithromycin, antagonized gentamycin and D-cycloserine, whereas they synergized with the tetracyclines, polymyxin B, DL-3-hydroxynorvaline, lamotrigine, and *p*-fluoro-phenylalanine.

(C) The thiopurines, 6-thioguanine and 6-mercaptopurine, are anticancer drugs that revealed highly overlapping signature interactions. All interactions were done in *E. coli* BW25113 grown in M9 minimal medium and were color coded as in Figure 1.

lamotrigine, as well as 6-mercaptopurine and aminoglycosides. Indeed, these interactions in particular revealed further insight into the complex metabolic network that underpins nutrient stress, as well as the connectivity with other biosynthetic pathways and cellular housekeeping functions.

Biotin Synthesis Interacts with Cell Wall, SAM, and Fatty Acid Biosynthesis

The biotin biosynthesis inhibitor MAC13772 targets 7,8-diaminopelargonic acid synthase (BioA), an enzyme responsible for the catalysis of the antepenultimate step in biotin biosynthesis (Zlitni et al., 2013). Its chemical interaction profile identified one antagonistic and four synergistic signature interactions (Figure 3A). MAC13772 antagonized the activity of the cell wall antibiotic D-cycloserine (FICI $\geq$3, Figure S3A), a D-alanine analog that competitively inhibits two essential enzymes, alanine racemase and D-alanine-D-alanine ligase (Lambert and Neuhaus, 1972; Zawadzke et al., 1991). The racemase catalyzes the conversion of L-alanine to D-alanine, and the ligase utilizes two D-alanine molecules as substrates for peptidoglycan synthesis (Figure S4). Notably, the biotin biosynthetic step preceding the antepenultimate step utilizes L-alanine as a substrate (Figure 3B). The observed antagonistic interaction suggests that the inhibition of BioA increases L-alanine availability from the preceding biotin biosynthetic step (Figure S3). Where L-alanine and D-cycloserine compete for binding to the active site of the racemase, the abundance of L-alanine enables alanine racemization and continued peptidoglycan synthesis, suppressing D-cycloserine's activity. Recent genomic analyses of *Mycobacterium tuberculosis* have revealed that strains harboring a loss-of-function mutation in *ald*, which codes for an enzyme that catalyzes the conversion of L-alanine to pyruvate, are resistant to D-cycloserine (Desjardins et al., 2016). This Ald variant can no longer utilize L-alanine as a substrate, leading to an increase in the pool of available L-alanine and suppression of D-cycloserine activity. Accordingly, we speculate that L-alanine is redirected toward peptidoglycan synthesis on inhibition of BioA and antagonizes the effects of D-cycloserine.

In addition to its connection to cell wall synthesis, the BioA inhibitor MAC13772 also synergized with L-norleucine (FICI $\leq$0.5), a nutrient synthesis probe that targets SAM biosynthesis (Chattopadhyay et al., 1991). In *E. coli*, the first biotin biosynthetic step requires SAM as a methyl donor (Figure 3B). L-norleucine inhibits the methionine adenosyltransferase reaction of the MetK enzyme that catalyzes the production of SAM

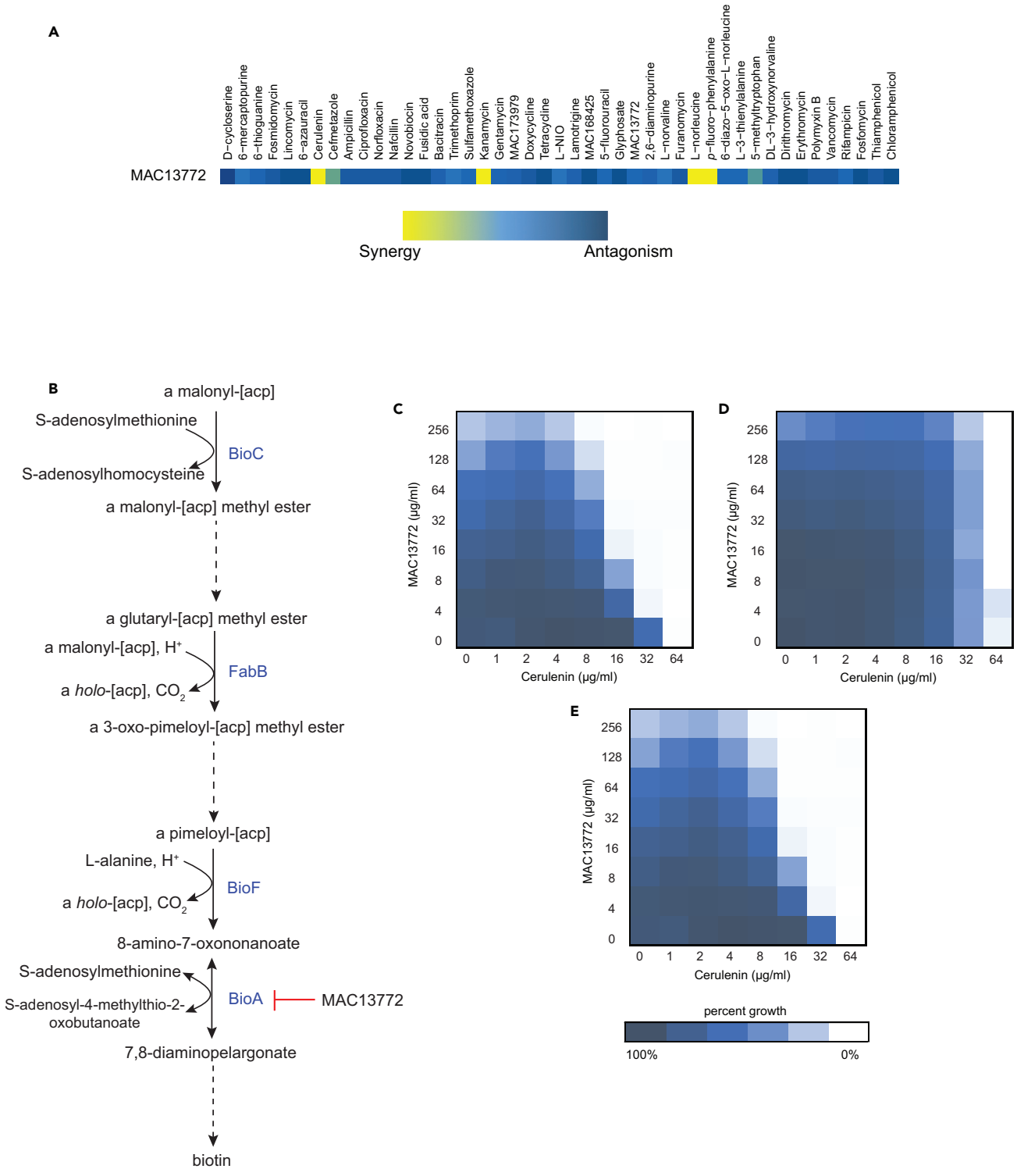

Figure 3. Synergy of MAC13772 with Cerulenin Reveals the Importance of Biotin Availability for Fatty Acid Biosynthesis

(A) The growth inhibitory interaction profile of MAC13772 with other probes. *E. coli* BW25113 was grown in M9 minimal medium. Interactions were color coded as in Figure 1.

(B) Biotin biosynthesis in *E. coli* requires S-adenosylmethionine (SAM) in its first committed step. FabB catalyzes one of the elongation steps. MAC13772 inhibits the antepenultimate step in biotin biosynthesis by targeting BioA. Dashed arrows represent more than one biosynthetic step.

Figure 3. *Continued*

(C) The synergistic interaction (FICI ≤0.5) of MAC13772 and cerulenin; *E. coli* BW25113 grown in M9 minimal medium.

(D) The synergistic interaction in (C) was suppressed (FICI ≤2) in nutrient-rich conditions; *E. coli* BW25113 grown in Luria-Bertani (LB) medium.

(E) The synergistic interaction (FICI ≤0.38) was also observed in the mutant strain *E. coli* BW25113 Δ*bioP* (Baba et al., 2006), lacking the biotin transporter, grown in LB medium. See also Figures S3 and S4.

(Chattopadhyay et al., 1991). Thus the first step of biotin biosynthesis is perturbed by the action of L-norleucine, and synergy is seen with MAC13772, an inhibitor of the antepenultimate step of the same pathway (Figure 3B). Indeed, it has been previously shown that inhibition of SAM-dependent methyltransferases cascades to the inhibition of biotin biosynthesis (Lin et al., 2010). Accordingly, in nutrient-limited conditions, inhibition of both SAM and a late step in the biotin biosynthetic pathway exerts a synergistic inhibition of biotin biosynthesis in *E. coli*, leading to growth inhibition.

The synergistic interaction of MAC13772 and the antibiotic cerulenin (FICI ≤0.5) highlighted an interdependence between biotin biosynthesis and fatty acid synthesis in nutrient-limited conditions (Figures 3C and 3D). Cerulenin targets ß-ketoacyl-ACP synthase I (FabB), one of the condensing enzymes required for fatty acid biosynthesis (Price et al., 2001) and one of the four enzymes involved in the elongation of biotin's saturated chain moiety (Figure 3B). The first step in *E. coli*'s fatty acid biosynthetic pathway is a decarboxylation reaction catalyzed by the acetyl-CoA carboxylase (ACC) complex, which uses biotin as a cofactor (Campbell and Cronan, 2001). Thus the inhibition of biotin biosynthesis appears to have a unique impact on fatty acid biosynthesis when *E. coli* is grown in nutrient-limited conditions. We assessed the effect of decreased biotin availability in nutrient-rich conditions using a Δ*bioP* mutant, harboring a deletion in the biotin transporter. In this genetic background, biotin biosynthesis becomes essential in nutrient-rich conditions. Indeed, Figure 3E revealed a synergistic interaction in the Δ*bioP* mutant strain, in which cerulenin was similarly potentiated in the presence of sub-inhibitory concentrations of MAC13772. Thus a decrease in biotin availability affects fatty acid biosynthesis and sensitizes this pathway to inhibition by the antibiotic cerulenin.

Perturbation of S-Adenosylmethionine Biosynthesis Reveals a Growth Phenotype for the Ribosome Biogenesis Function of Initiation Factor 2

Lamotrigine is best known as an anticonvulsant drug; however, it was recently shown to have the cryptic ability to inhibit a previously unrecognized ribosome biogenesis function in *E. coli*, namely, that of initiation factor 2 (IF2) (Stokes et al., 2014). While IF2 is understood to have a key role in the initiation of protein translation, its role in ribosome assembly was revealed through an investigation of the action of lamotrigine under conditions of cold stress (15°C). Indeed, the ability of lamotrigine to inhibit the growth of *E. coli* was dependent on cold stress. Herein, under nutrient-limited conditions and at 37°C, we found that lamotrigine showed a cold-independent activity, particularly in combination with certain compounds. The chemical interaction profile of lamotrigine revealed 12 synergistic interactions (Figure 4A), including those with the antibiotics cerulenin and rifampicin, which persisted in nutrient-rich conditions (Figure S5). Ribosome assembly remains a highly enigmatic process (Shajani et al., 2011). Indeed, we are at a loss to identify a precise mechanism behind many of the interactions that we observed for lamotrigine. Nevertheless, we believe that the synergistic interaction between the SAM biosynthesis inhibitor L-norleucine (Chattopadhyay et al., 1991) and lamotrigine (Figures 4B and 4C) may be instructive of the network that underpins ribosome assembly. Remarkably, inhibition of SAM biosynthesis revealed a growth inhibitory phenotype for the IF2-targeted compound lamotrigine under standard temperature conditions (37°C).

Ribosome profiling analysis, an assessment of the distribution of ribosomal material among the 30S, 50S, and 70S species using sucrose gradient sedimentation, is a signature phenotype that is commonly used to characterize defects in ribosome assembly. Treatment of *E. coli* growing in nutrient-rich media at 15°C with lamotrigine was previously shown to be growth inhibitory and lead to the accumulation of immature pre-30S and pre-50S ribosomal particles, consistent with its inhibition of ribosome biogenesis (Stokes et al., 2014). Lamotrigine treatment had no such impact on growth or ribosome profiles, however, when *E. coli* was grown in nutrient-rich media at 37°C. In the work reported herein, lamotrigine treatment at 15°C in nutrient-limited media revealed the accumulation of a pre-50S species only (Figure S6). Notably, this phenotype was also seen when cells grown at 37°C in nutrient-limited conditions were treated with lamotrigine. Ribosomal subunit assembly is not thought to proceed with a linear and specific maturation pathway. Instead, emerging research suggests that there are multiple and parallel pathways

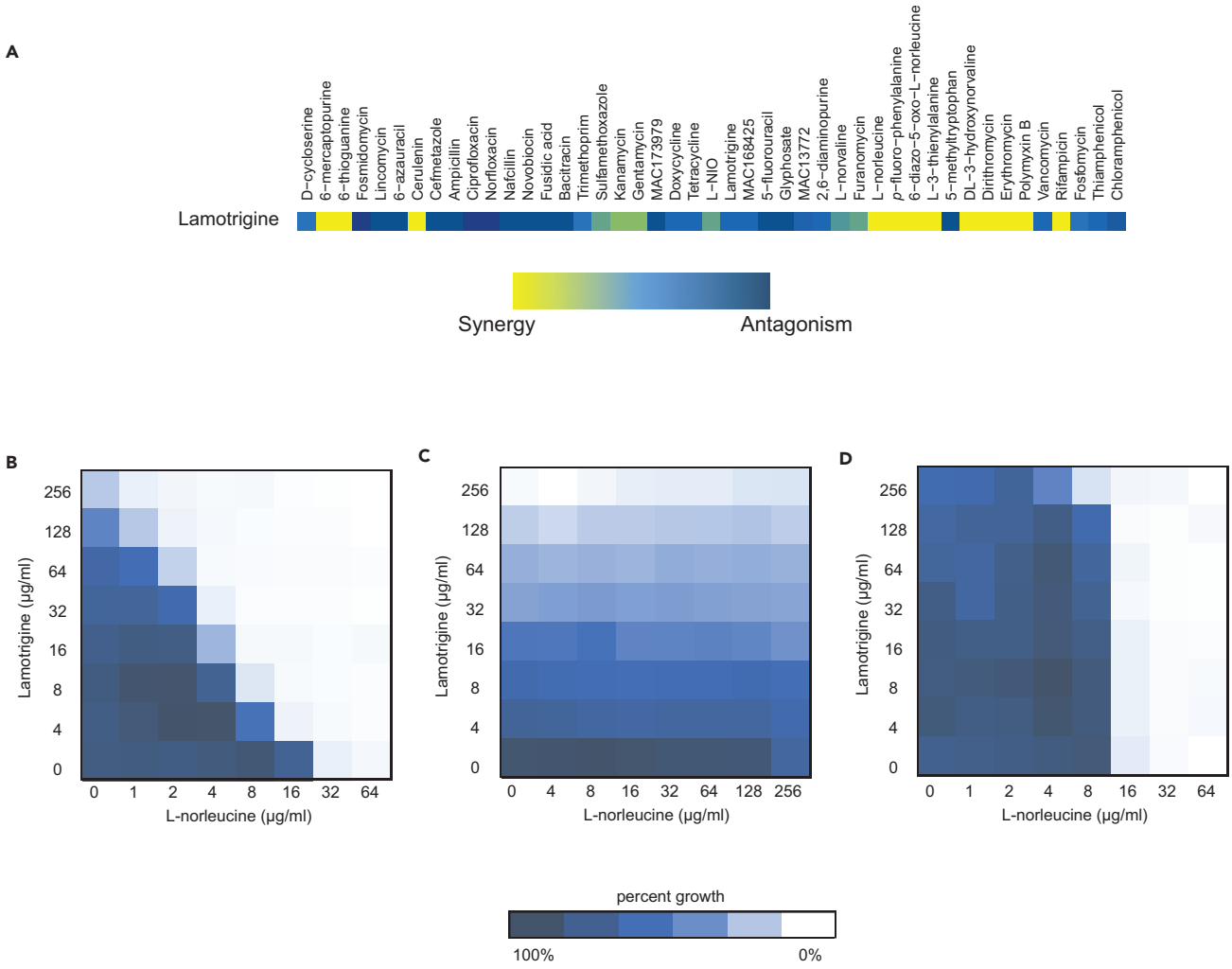

Figure 4. The Ribosome Biogenesis Function of IF2 is Revealed when S-Adenosylmethionine Biosynthesis is Perturbed

(A) The growth inhibitory interaction profile of lamotrigine with other probes. *E. coli* BW25113 grown in M9 minimal medium at 37°C. Interactions were color coded as in Figure 1.

(B) The synergistic interaction of lamotrigine with L-norleucine (FICI ≤0.25); *E. coli* BW25113 grown in M9 minimal medium.

(C) The synergistic interaction in (B) was suppressed (FICI ≤2) in nutrient-rich conditions; *E. coli* BW25113 grown in LB medium.

(D) The interaction of lamotrigine with L-norleucine using the *E. coli* IF2 mutant (Stokes et al., 2014) grown in M9 minimal medium (FICI ≤1.5). This panel provides evidence that it is the ribosome biogenesis function of IF2 that contributes to the synergy seen between lamotrigine and L-norleucine. See also Figures S5 and S6.

for maturation. Our earlier work with lamotrigine suggested that, whereas the function of IF2 in late ribosomal subunit assembly was dispensable at 37°C, it became essential at cold temperatures wherein alternative pathways for assembly became limiting due to the effect of temperature on RNA folding. Nutrient limitation has not made this function essential for growth—Figure 4B reveals that high concentrations of lamotrigine alone are not especially growth inhibitory—but has revealed a small but detectable defect in the ribosome profile. Here again we posit that nutrient limitation may limit the assembly landscape, revealing a dependence on IF2. Notwithstanding its interaction with lamotrigine in these conditions, L-norleucine-treated cells grown at 37°C in nutrient-limited conditions had a ribosome profile that was indistinguishable from those of untreated cells (Figure S6). Interestingly, SAM-dependent methylation of multiple sites of 30S and 50S ribosomal particles has a key role in ribosome biogenesis (Kaczanowska and Rydén-Aulin, 2007; Shajani et al., 2011). To be sure that this interaction was due to the inhibition of IF2's ribosome assembly function, we assessed the interaction with an *E. coli* IF2 mutant (mutant 1) (Stokes et al., 2014). This mutant encodes an N-terminal IF2 variant that resists the capacity of lamotrigine to inhibit

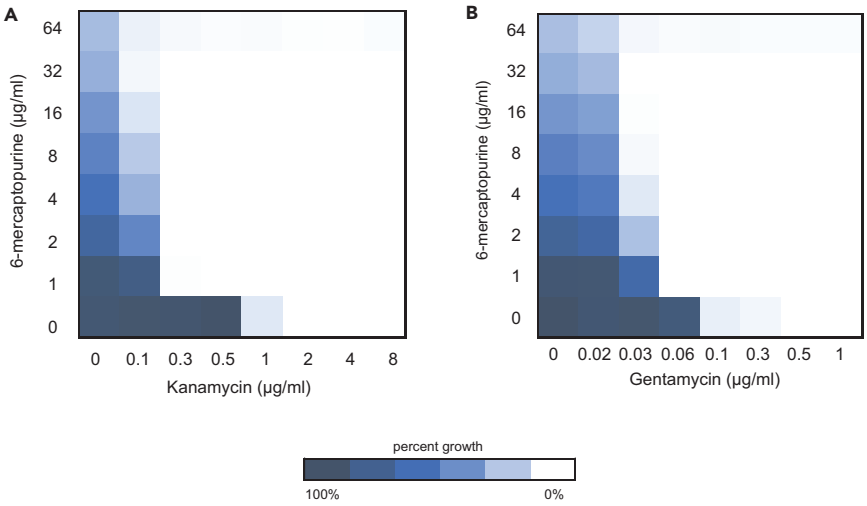

Figure 5. The Antimetabolite 6-Mercaptopurine Synergizes with Aminoglycoside Antibiotics

(A and B) The figure presents checkerboard assays to analyze the interaction between 6-mercatopurine and the aminoglycosides kanamycin and gentamycin in *E. coli* BW25113 grown in M9 minimal medium. The synergistic interaction between 6-mercaptopurine and (A) kanamycin has an FICI $\leq$0.27, whereas (B) gentamycin's interaction has an FICI $\leq$0.31. See also Figure S7.

the ribosome assembly activity of IF2. (We note here that lamotrigine does not affect the protein translation function of IF2.) The absence of synergy in Figure 4D confirmed that the interaction in wild-type *E. coli* was related to the role of IF2 in ribosome assembly. Although treatment of wild-type *E. coli* with L-norleucine did not produce immature ribosomal particles (Figure S6), perturbation of SAM biosynthesis with L-norleucine revealed a profound growth phenotype at 37°C for the ribosome biogenesis function of IF2.

Thiopurine Analogs Showed Synergy with Aminoglycoside Antibiotics

Thiopurine antagonists are known for their incorporation into DNA and RNA and for their inhibition of purine biosynthesis (Van Scoik et al., 1985). Two anticancer drugs, 6-thioguanine and 6-mercaptopurine, are thiopurine analogs that exhibit antibacterial activity in nutrient-defined media (Coonrod and Eickhoff, 1972; Elion et al., 1954b). The MOA of these drugs in both animal and bacterial cells is thought to be manifold. They are converted to purine analogs and get incorporated into DNA and RNA, but they also inhibit purine biosynthesis directly and through negative feedback mechanisms (Atkinson and Murray, 1965; Bolton and Mandel, 1957; Coggin et al., 1966; Elion et al., 1954a). These drugs showed relatively promiscuous interaction profiles in our study. For example, 10 synergistic interactions were seen for 6-mercaptopurine (Figure 2C). We posit that the central role of purine synthesis in metabolism and growth leads to pleiotropy and a high density of interactions for these probes. Nevertheless, we found it curious that, of the many protein synthesis inhibitors studied, we saw interactions with only the aminoglycoside class, namely, with kanamycin and gentamycin. We followed up on this observation, focusing on the probe 6-mercaptopurine (Figure 5) because it was more potent than 6-thioguanine (Figure S7). Aminoglycoside antibiotics are understood to corrupt ribosome function by promoting mistranslation of proteins, and these have toxic effects (Davies et al., 1965). Aminoglycosides encompass two distinct structural classes, the 4,5-disubstituted and the 4,6-disubsituted 2-deoxystreptamines, and a structurally dissimilar class that does not share a common backbone in their chemical structures (Mingeot-Leclercq et al., 1999; Recht and Puglisi, 2001). In the course of interfering with ribosome function, these compounds form sequence-specific hydrogen bonds with nucleotides in the 30S ribosome subunit (Recht and Puglisi, 2001). We reasoned that if 6-mercaptopurine was incorporated into RNA, then it may exert synergy with aminoglycosides through specific interactions. We found that 6-mercaptopurine showed strong synergy not only with the 4,6-disusbtituted aminoglycosides kanamycin and gentamycin but also with all aminoglycosides tested regardless of the structural class (Figure 6). Thus we conclude that the synergy is not due to specific interactions but rather due to the downstream consequences of inhibition of purine biosynthesis and/or incorporation into DNA and RNA. Notably, neomycin resulted in the strongest synergistic interaction profile in which 6-mercaptopurine was potentiated by more than 100-fold (Figure 6A). In all, these findings revealed an

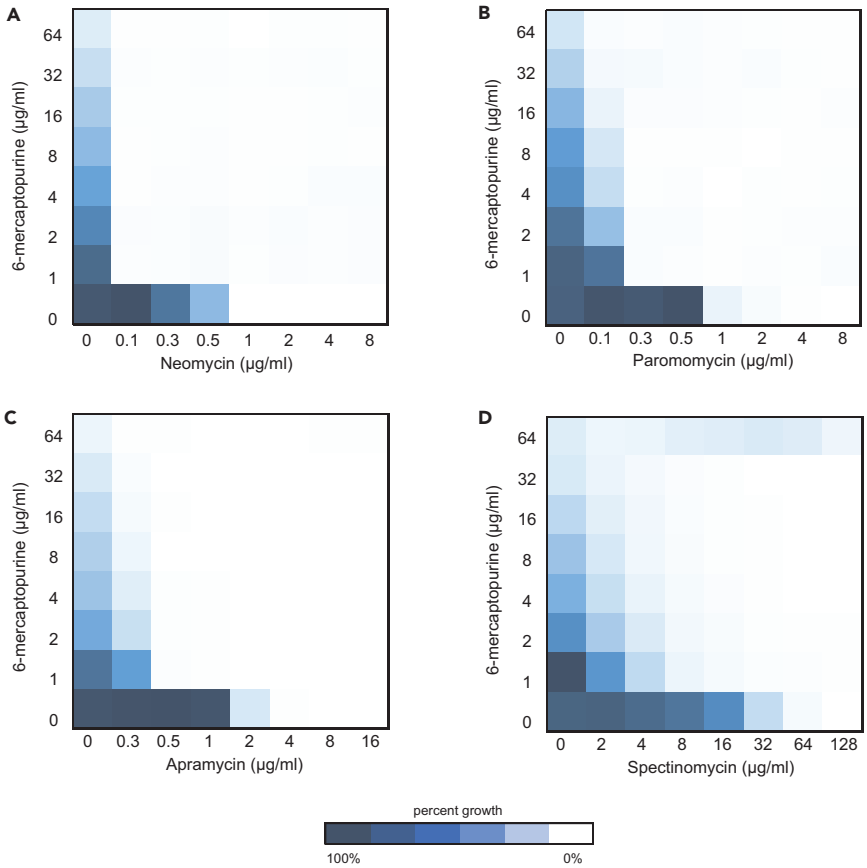

Figure 6. Analysis of the Interaction of 6-Mercaptopurine with a Panel of Structurally Diverse Aminoglycosides

(A–D) The figure presents checkerboard assays in *E. coli* BW25113 grown in M9 minimal medium to study the interaction of 6-meracptopurine with the 4,5-disubstituted 2-deoxystreptamine aminoglycosides (A) neomycin (FICI $\leq$0.14) and (B) paromomycin (FICI $\leq$0.14), as well as the structurally dissimilar class of aminoglycosides (C) apramycin (FICI $\leq$0.15) and (D) spectinomycin (FICI $\leq$0.14). See also Figure S7.

enigmatic interplay among (poly)nucleotide biosynthesis and the action of aminoglycosides on protein mistranslation.

DISCUSSION

Systematic mutation of *E. coli*'s genome of nearly 4,400 genes has revealed that some 303 genes are essential for growth in nutrient-rich conditions. These genes code for the so-called housekeeping functions in the bacteria, which include cell wall, DNA, RNA, and protein synthesis. Under nutrient stress, an additional set of 119 genes have an indispensable phenotype and these genes code largely for the synthesis of amino acids, vitamins, nucleobases, and other cofactors. While much is known about the function of this set of 422 genes and their gene products, relatively little is known of their interactions. Gene-gene interactions are commonly studied in model microbes with systematic genome-wide crosses of deletion mutations to detect unexpected growth defects in strains bearing deletions in two otherwise dispensable genes, resulting in a synthetic lethal or sick phenotype (Butland et al., 2008; Collins et al., 2007; Costanzo et al., 2016; Côté et al., 2016; Tong et al., 2001; Typas et al., 2008). To date, this approach has been limited, in *E. coli*, to the dispensable fraction of the genome where stable mutants can be created. Herein, we sought to probe the collection of genes involved in both housekeeping and nutrient stress functions (422) under conditions wherein they have an essential growth phenotype. To this end, we systematically combined 45 chemical probes targeting a subset of these functions. The 45 compounds included 18 nutrient synthesis probes with growth inhibitory activities restricted to nutrient-limited conditions and 27 housekeeping-function probes that included antibiotics that target cell wall, protein synthesis, or DNA replication and lamotrigine,

a compound that was recently identified to be an inhibitor of bacterial ribosome biogenesis (Stokes et al., 2014).

The binary combination space for these 45 compounds encompasses 990 unique pairwise chemical-chemical combinations. Of these systematic combinations, we mapped 186 interactions, of which 81 were synergistic and 105 were antagonistic. In addition, we defined signature interaction profiles for all 45 compounds under nutrient stress conditions, averaging 4 interactions per compound. Thus 19% (186/990) of probe combinations produced an interaction in this study. This number is high relative to the 3.5% frequency recorded in the model yeast for both positive and negative gene-gene interactions seen genome-wide in that organism (Costanzo et al., 2016). Indeed, synthetic lethal/sick interactions recorded among the dispensable fraction in *E. coli* have been in a similar frequency range, for example, ~1% of the total number of double mutants created (French et al., 2017). Interestingly, interactions among the essential gene set in the model yeast *S. cerevisiae* have been probed using temperature-sensitive alleles (Costanzo et al., 2016) and this work has revealed a much higher frequency of interaction (24%), closer to that seen here using chemical probes of essential functions. Together, these studies suggest that essential physiology is described by a network that is much more densely wired than that of the dispensable fraction.

Hierarchical clustering of these 45 chemical-chemical interaction profiles revealed that compounds clustered based on their chemical class. This points to a qualitative dataset since analogs share a similar MOA, thus resulting in overlapping interaction profiles. Indeed, drugs belonging to the same antibiotic class clustered together, revealing the least dissimilarity in their signature interactions. Another cluster identified highly similar profiles between the nutrient synthesis probes 6-thioguanine and 6-mercaptopurine. Occasionally, some interaction profiles clustered due to a shared synergistic interaction between the two clustered compounds. This phenotype occurred for increasingly dissimilar interaction profiles, suggesting that the interaction matrix is not predictive of synergistic interactions. Rather, the chemical-chemical interaction matrix is a powerful tool that can be used to elucidate the MOA of novel compounds with antibacterial activity (unknowns). Particularly, unknowns with a growth inhibitory activity restricted to nutrient-limited conditions can have their target prioritized through nutrient suppression profiling (Zlitni et al., 2013), in which unknowns selectively targeting a unique nutrient biosynthetic pathway are suppressed in the presence of the respective nutrient. However, nutrient suppression profiling lacks the ability to determine the target of unknowns suppressed by multiple nutrients. We have previously demonstrated the utility of chemical combinations in elucidating the target and MOA of uncharted chemical probes (Farha and Brown, 2010). Therefore, chemically combining the 45 compounds with such unknowns would generate fingerprint chemical interaction profiles that are unique to each unknown. Since the chemical-chemical interaction matrix clusters compounds with a similar MOA, hierarchical clustering of the unknowns' interaction profiles with that of the 45 compounds would allow the generation of testable hypotheses for the MOA of the unknown in question.

Systematic combinations of nutrient synthesis probes and other bioactive compounds charted 186 interactions in *E. coli* grown in nutrient-limited conditions. Of the 186 interactions, 57 involved combinations of housekeeping-function probes, many of which have been identified by previous antibiotic combination studies (Ocampo et al., 2014; Wambaugh et al., 2017; Yeh et al., 2006). Herein, we report a novel synergistic interaction in *E. coli* that involves the Gram-positive antibiotic novobiocin and the cell wall-active antibiotic fosmidomycin. This was an interesting observation in which a Gram-positive antibiotic was potentiated in *E. coli*, a Gram-negative bacterium. Nevertheless, we focused herein on interactions that provide further understanding of nutrient stress in *E. coli*. Of the 129 interactions, we prioritized three interactions to understand the connectivity between nutrient synthesis and other cellular housekeeping functions in nutrient-limited conditions.

Combinations of nutrient synthesis probes revealed how biosynthetic pathways are interdependent in nutrient-limited conditions. Previous *in vitro* studies have shown that inhibition of fatty acid biosynthesis by cerulenin perturbs biotin biosynthesis (Lin et al., 2010). In this work, we report a synergistic interaction between the biotin biosynthesis inhibitor, MAC13772, and cerulenin. Furthermore, this synergy echoes a synthetic sick interaction observed between *fabH*, coding for a fatty acid biosynthetic enzyme, and *bioA*, encoding the target in biotin synthesis for the compound MAC13772 (Côté et al., 2016). Together these studies suggest a strong connectivity between these biosynthetic pathways. To further probe this connectivity, we assessed the interaction between MAC13772 and cerulenin in nutrient-rich conditions,

and in an *E. coli* strain (Δ*bioP)* lacking the biotin transporter, making biotin biosynthesis essential regardless of the growth medium. Here again, we saw a strong interaction between these compounds consistent with a crucial role for the biotin biosynthetic pathway in the synthesis of fatty acids.

Other interactions that we studied in detail were those of lamotrigine, an inhibitor of the ribosome biogenesis function of IF2 (IF2) in *E. coli* (Stokes et al., 2014). Lamotrigine proved to be a promiscuous interactor with 12 novel synergistic partner compounds. The activity of lamotrigine against IF2 has formerly only been evident under cold stress, a condition that is thought to narrow the complex and redundant landscape for ribosomal subunit maturation. Thus the activity and cold-independent phenotype of lamotrigine in combination with several other cellular probes at 37°C is a new development and may be an indication that ribosome biogenesis is a particularly important hub in the cellular network. Of the 12 synergistic interactions, those with cerulenin and rifampicin were also evident in nutrient-rich media. Such interactions of clinically used drugs are intriguing from the prospect of therapy. In this context, we note that our dataset also revealed the well-known interaction between sulfamethoxazole and trimethoprim, a highly synergistic interaction between sulfamethoxazole, an inhibitor of folate synthesis, and trimethoprim, an inhibitor of dihydrofolate reductase. The former is active only in nutrient-limited media, whereas the latter is active in both nutrient-limited and rich microbiological media, and arguably inhibits a housekeeping function, namely, the provision of reduced folates for a variety of cellular processes including DNA synthesis. The mechanism behind this synergistic interaction, which persists in rich microbiological media, remains elusive, but is an example of one that has had great utility in antimicrobial therapy for many decades (Masters et al., 2003).

The interaction of lamotrigine with L-norleucine, an inhibitor of SAM biosynthesis was particularly interesting and consistent with the emerging recognition of the role of a number of bacterial methyltransferases in ribosome biogenesis (Baldridge and Contreras, 2014). The exact function of these modifications has been elusive; however, it has been suggested that methylation may serve as a checkpoint in ribosomal subunit assembly. The strong synergistic interaction seen in the work reported here sheds additional light on the role of IF2 in ribosome assembly by charting a connection between subunit methylation and the role of IF2 in the late steps of ribosome assembly. Of practical note, SAM biosynthesis has recently been identified as a potential antibacterial target in *M. tuberculosis*, where strains harboring SAM biosynthetic gene deletions are impaired for growth *in vivo* (Berney et al., 2015).

Another notable synergy was that between 6-mercaptopurine and aminoglycoside antibiotics. The former is an antimetabolite used in cancer therapy but not for bacterial infection. Although the precise mechanism underpinning the synergy remains unknown, we present evidence herein that the synergy is not due to the direct interaction of aminoglycosides with thiopurines incorporated into ribosomal RNA. Where purine biosynthesis has been shown to be important for the proliferation and survival of *E. coli* in blood (Samant et al., 2008), the interaction with aminoglycosides is one worthy of additional study, as is the potential of combination therapies that would exploit targets in translation and purine synthesis.

The chemical biology combinations approach reported herein has charted the first foray into pairwise interactions of functions in *E. coli* with essential growth phenotypes. The effort defined a high density of interactions among these functions and suggests that additional probes would facilitate the expansion of this effort to further understand this aspect of the bacterial cell network as well as the importance of nutrient stress. Indeed, nutrient metabolism is emerging as a viable virulence target in pathogenic bacteria (Cersini et al., 1998; Cuccui et al., 2007; Mei et al., 1997). Full validation of nutrient metabolism as a therapeutic target will come from studies of sites of infection and specific pathogens as well as a thorough understanding of the complex network that underpins nutrient stress in bacteria.

METHODS

All methods can be found in the accompanying Transparent Methods supplemental file.

SUPPLEMENTAL INFORMATION

Supplemental Information includes Transparent Methods, seven figures, and two data files and can be found with this article online at https://doi.org/10.1016/j.isci.2018.03.018.

ACKNOWLEDGMENTS

This work was supported by a salary award to E.D.B. from the Canada Research Chairs program as well as by an operating funding from the Canadian Institutes of Health Research [FDN-143215]. We thank Gerard D. Wright for providing the natural product furanomycin. We also thank Maya A. Farha for the helpful suggestions and comments on the manuscript and Jonathan M. Stokes for the insightful discussions on ribosome biogenesis.

AUTHOR CONTRIBUTIONS

Conceptualization, S.S.E. and E.D.B.; methodology, S.S.E. and E.D.B.; software, S.S.E.; validation, S.S.E.; formal analysis, S.S.E.; investigation, S.S.E. and E.D.B.; resources, E.D.B.; writing: original draft, S.S.E. and E.D.B.; writing: review and editing, S.S.E. and E.D.B.; visualization, S.S.E.; supervision, E.D.B.; funding acquisition, E.D.B.

DECLARATION OF INTERESTS

The authors declare no competing interests.

Received: December 19, 2017
Revised: February 28, 2018
Accepted: March 7, 2018
Published: April 27, 2018

REFERENCES

Atkinson, M.R., and Murray, A.W. (1965). Inhibition by 6-mercaptopurine of purine phosphoribosyltransferases from Ehrlich ascites-tumour cells that are resistant to this drug. Biochem. J. *94*, 71–74.

Baba, T., Ara, T., Hasegawa, M., Takai, Y., Okumura, Y., Baba, M., Datsenko, K.A., Tomita, M., Wanner, B.L., and Mori, H. (2006). Construction of *Escherichia coli* K-12 in-frame, single-gene knockout mutants: the Keio collection. Mol. Syst. Biol. *2*, 2006.0008.

Baldridge, K.C., and Contreras, L.M. (2014). Functional implications of ribosomal RNA methylation in response to environmental stress. Crit. Rev. Biochem. Mol. Biol. *49*, 69–89.

Berney, M., Berney-Meyer, L., Wong, K.-W., Chen, B., Chen, M., Kim, J., Wang, J., Harris, D., Parkhill, J., Chan, J., et al. (2015). Essential roles of methionine and S-adenosylmethionine in the autarkic lifestyle of *Mycobacterium tuberculosis*. Proc. Natl. Acad. Sci. USA *112*, 10008–10013.

Bolton, E.T., and Mandel, H.G. (1957). The effects of 6-mercaptopurine on biosynthesis in *Escherichia coli*. J. Biol. Chem. *227*, 833–844.

Butland, G., Babu, M., Diaz-Mejia, J.J., Bohdana, F., Phanse, S., Gold, B., Yang, W., Li, J., Gagarinova, A.G., Pogoutse, O., et al. (2008). eSGA: *E. coli* synthetic genetic array analysis. Nat. Methods *5*, 789–795.

Campbell, J.W., and Cronan, J.E., Jr. (2001). Bacterial fatty acid biosynthesis: targets for antibacterial drug discovery. Annu. Rev. Microbiol. *55*, 305–332.

Cersini, A., Salvia, A.M., and Bernardini, M.L. (1998). Intracellular multiplication and virulence of *Shigella flexneri* auxotrophic mutants. Infect. Immun. *66*, 549–557.

Chattopadhyay, M.K., Ghosh, A.K., and Sengupta, S. (1991). Control of methionine biosynthesis in *Escherichia coli* K-12: a closer study with analogue-resistant mutants. J. Gen. Microbiol. *137*, 685–691.

Coggin, J.H., Loosemore, M., and Martin, W.R. (1966). Metabolism of 6-mercaptopurine by resistant *Escherichia coli* cells. J. Bacteriol. *92*, 446–454.

Collins, S.R., Miller, K.M., Maas, N.L., Roguev, A., Fillingham, J., Chu, C.S., Schuldiner, M., Gebbia, M., Recht, J., Shales, M., et al. (2007). Functional dissection of protein complexes involved in yeast chromosome biology using a genetic interaction map. Nature *446*, 806–810.

Coonrod, J.D., and Eickhoff, T.C. (1972). Combined action of 6-mercaptopurine and antibiotics on gram-negative bacteria *in vitro*. Proc. Soc. Exp. Biol. Med. *140*, 524–527.

Costanzo, M., VanderSluis, B., Koch, E.N., Baryshnikova, A., Pons, C., Tan, G., Wang, W., Usaj, M., Hanchard, J., Lee, S.D., et al. (2016). A global genetic interaction network maps a wiring diagram of cellular function. Science *353*, aaf1420.

Côté, J.P., French, S., Gehrke, S.S., MacNair, C.R., Mangat, C.S., Bharat, A., and Brown, E.D. (2016). The genome-wide interaction network of nutrient stress genes in *Escherichia coli*. MBio *7*, e01714–16.

Cozzarelli, N.R. (1977). The mechanism of action of inhibitors of DNA synthesis. Annu. Rev. Biochem. *46*, 641–668.

Cuccui, J., Easton, A., Chu, K.K., Bancroft, G.J., Oyston, P.C.F., Titball, R.W., and Wren, B.W. (2007). Development of signature-tagged mutagenesis in *Burkholderia pseudomallei* to identify genes important in survival and pathogenesis. Infect. Immun. *75*, 1186–1195.

Davies, J., Gorini, L., and Davis, B.D. (1965). Misreading of RNA codewords induced by aminoglycoside antibiotics. Mol. Pharmacol. *1*, 93–106.

Desjardins, C.A., Cohen, K.A., Munsamy, V., Abeel, T., Maharaj, K., Walker, B.J., Shea, T.P., Almeida, D.V., Manson, A.L., Salazar, A., et al. (2016). Genomic and functional analyses of *Mycobacterium tuberculosis* strains implicate *ald* in D-cycloserine resistance. Nat. Genet. *48*, 544–551.

Drlica, K., Malik, M., Kerns, R.J., and Zhao, X. (2008). Quinolone-mediated bacterial death. Antimicrob. Agents Chemother. *52*, 385–392.

Elion, G.B., Bieber, S., and Hitchings, G.H. (1954a). The fate of 6-mercaptopurine in mice. Ann. N. Y. Acad. Sci. *60*, 297–303.

Elion, G.B., Singer, S., and Hitchings, G.H. (1954b). Microbiological effects of 6-mercaptopurine. Ann. N. Y. Acad. Sci. *60*, 200–206.

Farha, M.A., and Brown, E.D. (2010). Chemical probes of *Escherichia coli* uncovered through chemical-chemical interaction profiling with compounds of known biological activity. Chem. Biol. *17*, 852–862.

French, S., Côté, J.P., Stokes, J.M., Truant, R., and Brown, E.D. (2017). Bacteria getting into shape: genetic determinants of *E. coli* morphology. MBio *8*, e01977–e02016.

Joyce, A.R., Reed, J.L., White, A., Edwards, R., Osterman, A., Baba, T., Mori, H., Lesely, S.A., Palsson, B.Ø., and Agarwalla, S. (2006). Experimental and computational assessment of conditionally essential genes in *Escherichia coli*. J. Bacteriol. *188*, 8259–8271.

Kaczanowska, M., and Rydén-Aulin, M. (2007). Ribosome biogenesis and the translation process

in *Escherichia coli*. Microbiol. Mol. Biol. Rev. *71*, 477–494.

Keith, C.T., Borisy, A.A., and Stockwell, B.R. (2005). Multicomponent therapeutics for networked systems. Nat. Rev. Drug Discov. *4*, 71–78.

Krogstad, D., Moellering, R.J., and Lorian, V. (1986). Antibiotics in Laboratory Medicine (Williams and Wilkins).

Lambert, M.P., and Neuhaus, F.C. (1972). Mechanism of D-cycloserine action: alanine racemase from *Escherichia coli* W. J. Bacteriol. *110*, 978–987.

Li, Z., Vizeacoumar, F.J., Bahr, S., Li, J., Warringer, J., Vizeacoumar, F.S., Min, R., VanderSluis, B., Bellay, J., DeVit, M., et al. (2011). Systematic exploration of essential yeast gene function with temperature-sensitive mutants. Nat. Biotechnol. *29*, 361–367.

Lin, S., Hanson, R.E., and Cronan, J.E. (2010). Biotin synthesis begins by hijacking the fatty acid synthetic pathway. Nat. Chem. Biol. *6*, 682–688.

Masters, P.A., O'Bryan, T.A., Zurlo, J., Miller, D.Q., and Joshi, N. (2003). Trimethoprim-sulfamethoxazole revisited. Arch. Intern. Med. *163*, 402–410.

Mei, J.M., Nourbakhsh, F., Ford, C.W., and Holden, D.W. (1997). Identification of *Staphylococcus aureus* virulence genes in a murine model of bacteraemia using signature-tagged mutagenesis. Mol. Microbiol. *26*, 399–407.

Menninger, J.R., and Otto, D.P. (1982). Erythromycin, carbomycin, and spiramycin inhibit protein synthesis by stimulating the dissociation of peptidyl-tRNA from ribosomes. Antimicrob. Agents Chemother. *21*, 811–818.

Minajigi, A., Deng, B., and Francklyn, C.S. (2011). Fidelity escape by the unnatural amino acid β-hydroxynorvaline: an efficient substrate for *Escherichia coli* threonyl-tRNA synthetase with toxic effects on growth. Biochemistry *50*, 1101–1109.

Mingeot-Leclercq, M.-P., Glupczynski, Y., and Tulkens, P.M. (1999). Aminoglycosides: activity and resistance. Antimicrob. Agents Chemother. *43*, 727–737.

Nelson, J.A., Carpenter, J.W., Rose, L.M., and Adamson, D.J. (1975). Mechanisms of action of 6-thioguanine, 6-mercaptopurine, and 8-azaguanine. Cancer Res. *35*, 2872–2878.

Nichols, R.J., Sen, S., Choo, Y.J., Beltrao, P., Zietek, M., Chaba, R., Lee, S., Kazmierczak, K.M., Lee, K.J., Wong, A., et al. (2011). Phenotypic landscape of a bacterial cell. Cell *144*, 143–156.

Ocampo, P.S., Lázár, V., Papp, B., Arnoldini, M., Abel zur Wiesch, P., Busa-Fekete, R., Fekete, G., Pál, C., Ackermann, M., and Bonhoeffer, S. (2014). Antagonism between bacteriostatic and bactericidal antibiotics is prevalent. Antimicrob. Agents Chemother. *58*, 4573–4582.

Parsons, A.B., Brost, R.L., Ding, H., Li, Z., Zhang, C., Sheikh, B., Brown, G.W., Kane, P.M., Hughes, T.R., and Boone, C. (2004). Integration of chemical-genetic and genetic interaction data links bioactive compounds to cellular target pathways. Nat. Biotechnol. *22*, 62–69.

Price, A.C., Choi, K.-H., Heath, R.J., Li, Z., White, S.W., and Rock, C.O. (2001). Inhibition of β-ketoacyl-acyl carrier protein synthases by thiolactomycin and cerulenin: structure and mechanism. J. Biol. Chem. *276*, 6551–6559.

Recht, M.I., and Puglisi, J.D. (2001). Aminoglycoside resistance with homogeneous and heterogeneous populations of antibiotic-resistant ribosomes. Antimicrob. Agents Chemother. *45*, 2414–2419.

Samant, S., Lee, H., Ghassemi, M., Chen, J., Cook, J.L., Mankin, A.S., and Neyfakh, A.A. (2008). Nucleotide biosynthesis is critical for growth of bacteria in human blood. PLoS Pathog. *4*, e37.

Shajani, Z., Sykes, M.T., and Williamson, J.R. (2011). Assembly of bacterial ribosomes. Annu. Rev. Biochem. *80*, 501–526.

Stokes, J.M., Davis, J.H., Mangat, C.S., Williamson, J.R., and Brown, E.D. (2014). Discovery of a small molecule that inhibits bacterial ribosome biogenesis. Elife *3*, e03574.

Tong, A.H.Y., Evangelista, M., Parsons, A.B., Xu, H., Bader, G.D., Pagé, N., Robinson, M., Raghibizadeh, S., Hogue, C.W., Bussey, H., et al. (2001). Systematic genetic analysis with ordered arrays of yeast deletion mutants. Science *294*, 2364–2368.

Typas, A., Nichols, R.J., Siegele, D.A., Shales, M., Collins, S.R., Lim, B., Braberg, H., Yamamoto, N., Takeuchi, R., Wanner, B.L., et al. (2008). High-throughput, quantitative analyses of genetic interactions in *E. coli*. Nat. Methods *5*, 781–787.

Van Scoik, K.G., Johnson, C.A., and Porter, W.R. (1985). The pharmacology and metabolism of the thiopurine drugs 6-mercaptopurine and azathioprine. Drug Metab. Rev. *16*, 157–174.

Wambaugh, M.A., Shakya, V.P.S., Lewis, A.J., Mulvey, M.A., and Brown, J.C.S. (2017). High-throughput identification and rational design of synergistic small-molecule pairs for combating and bypassing antibiotic resistance. PLoS Biol. *15*, e2001644.

Yeh, P., Tschumi, A.I., and Kishony, R. (2006). Functional classification of drugs by properties of their pairwise interactions. Nat. Genet. *38*, 489–494.

Zawadzke, L.E., Bugg, T.D.H., and Walsh, C.T. (1991). Existence of two D-alanine:D-alanine ligases in *Escherichia coli*: cloning and sequencing of the *ddlA* gene and purification and characterization of the DdlA and DdlB enzymes. Biochemistry *30*, 1673–1682.

Zlitni, S., Ferruccio, L.F., and Brown, E.D. (2013). Metabolic suppression identifies new antibacterial inhibitors under nutrient limitation. Nat. Chem. Biol. *9*, 796–804.

ISCI, Volume *2*

Supplemental Information

Chemical-Chemical Combinations Map Uncharted Interactions in *Escherichia coli* under Nutrient Stress

Sara S. El Zahed and Eric D. Brown

Supplemental Figures and Figure Legends

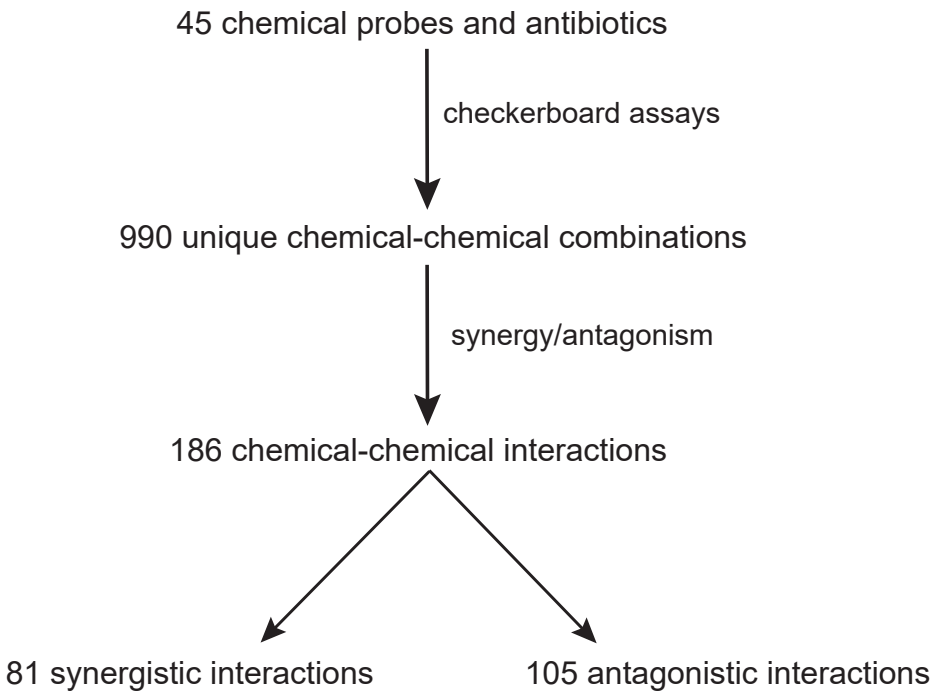

Figure S1. Summary of the Results from the Systematic Combination of 45 Compounds against *E. coli* BW25113. Related to Figure 1.

Through checkerboard assays, the chemical-chemical combination of 45 compounds against *E. coli* BW25113 grown in M9 minimal medium (0.4% glucose) resulted in more than 63,000 combination wells, constituting 990 unique chemical-chemical combinations. Of the 990 combinations, 81 were synergistic and 105 were antagonistic.

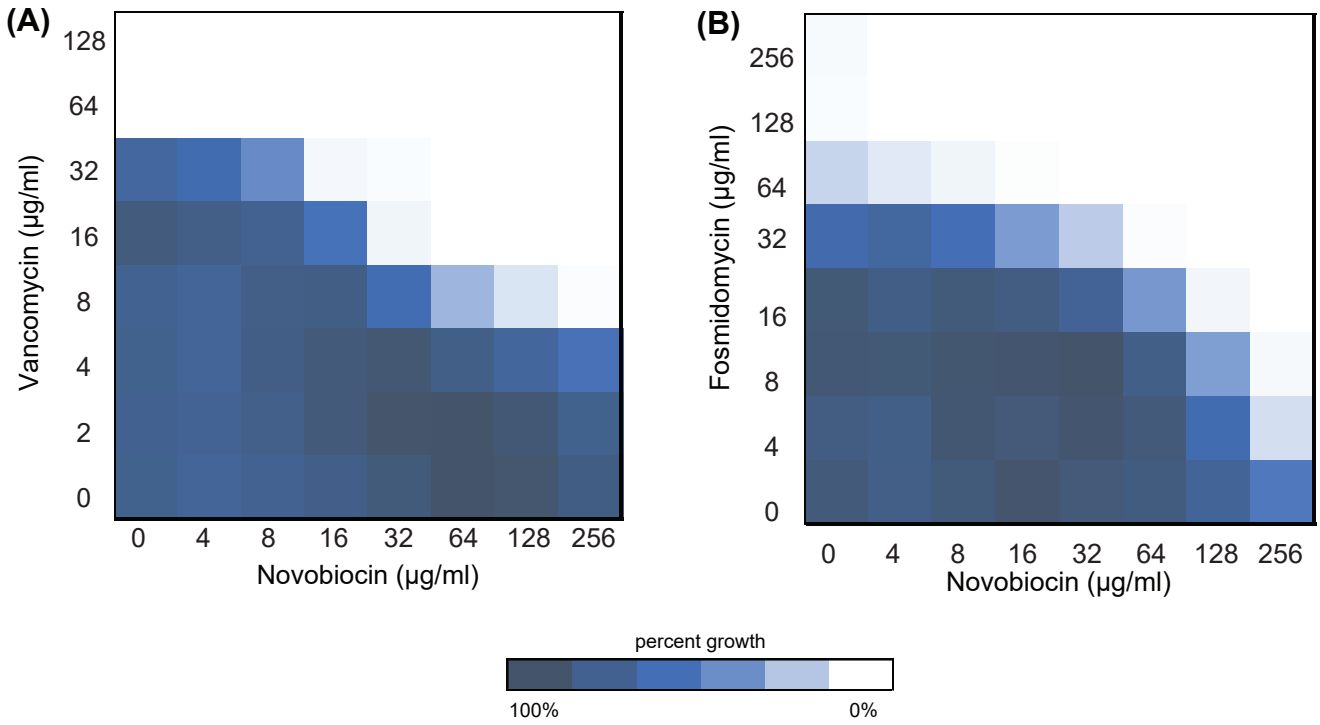

Figure S2. Novobiocin is Potentiated by Two Cell Wall Inhibitors. Related to Figure 1.
In *E. coli* BW25113 grown in M9 minimal medium (0.4% glucose), novobiocin is potentiated by both **(A)** vancomycin, FICI ≤ 0.38, and **(B)** fosmidomycin, FICI ≤ 0.5.

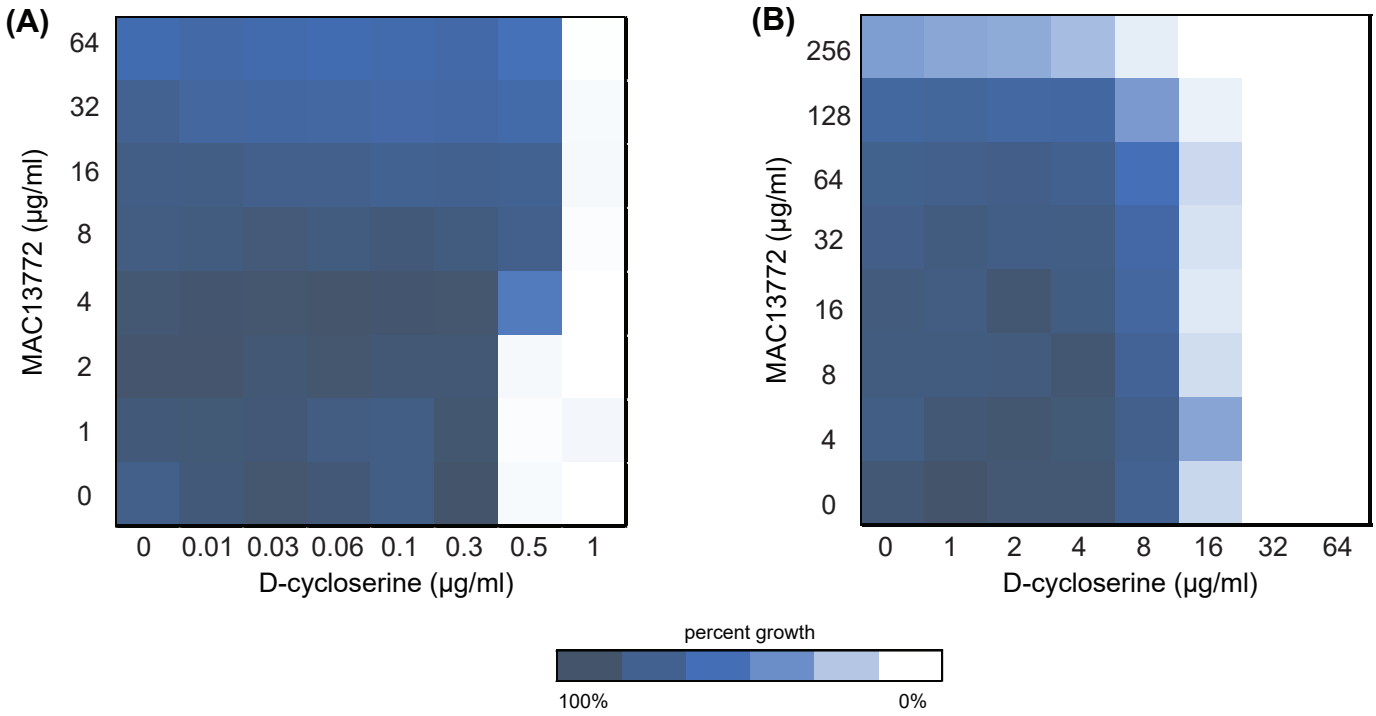

Figure S3. MAC13772 Antagonizes D-cycloserine in *E. coli* under Nutrient-Limited Conditions. Related to Figure 3.

(A) MAC13772's inhibition of biotin biosynthesis antagonizes D-cycloserine's growth inhibitory activity in *E. coli* under nutrient stress (FICI ≥ 3). **(B)** In nutrient-rich conditions, biotin biosynthesis is no longer required, thus suppressing MAC13772's antagonism of D-cycloserine (FICI ≤ 1).

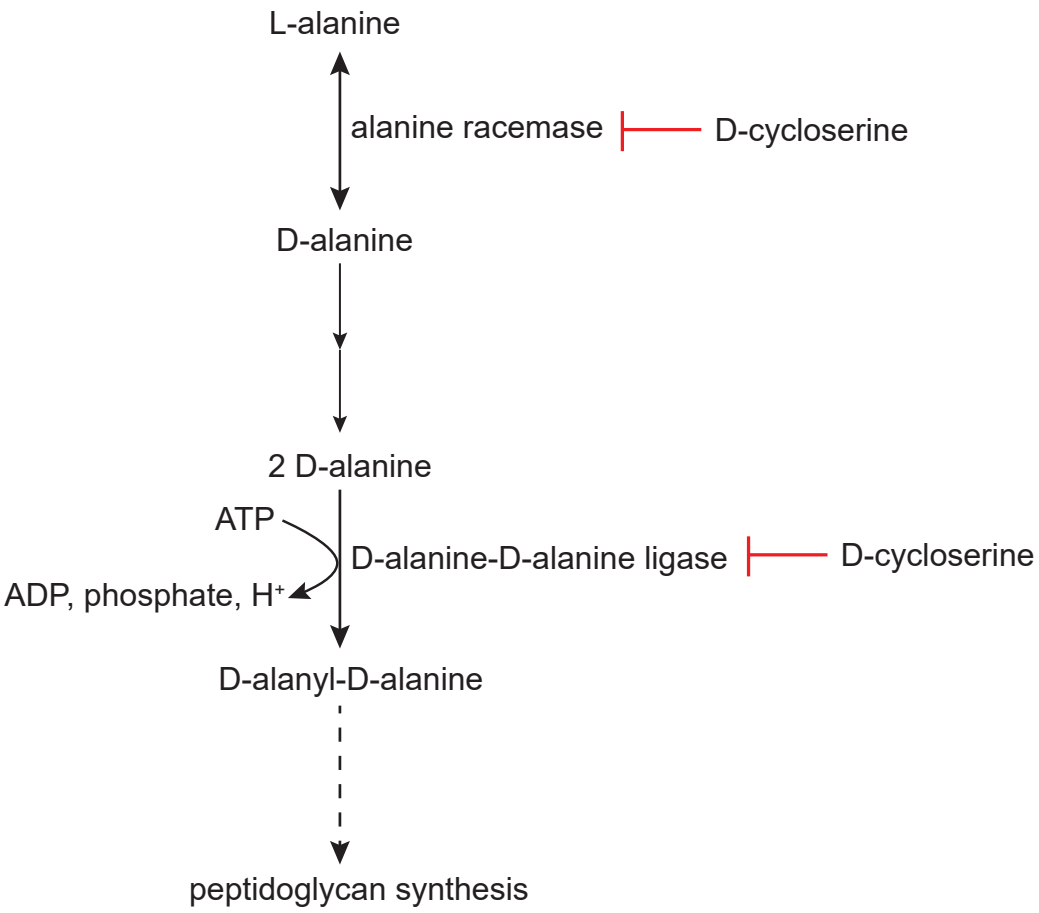

Figure S4. Summary of L-alanine Racemization for Peptidoglycan Biosynthesis in *E. coli*. Related to Figure 3.

L-alanine is converted to D-alanine, and two molecules of D-alanine are required by D-alanine-D-alanine ligase for peptidoglycan biosynthesis. D-cycloserine inhibits both enzymes. Two consecutive arrows are used to indicate that two D-alanine molecules need to be synthesized for the ligase. Dashed arrow represents more than one biosynthetic step.

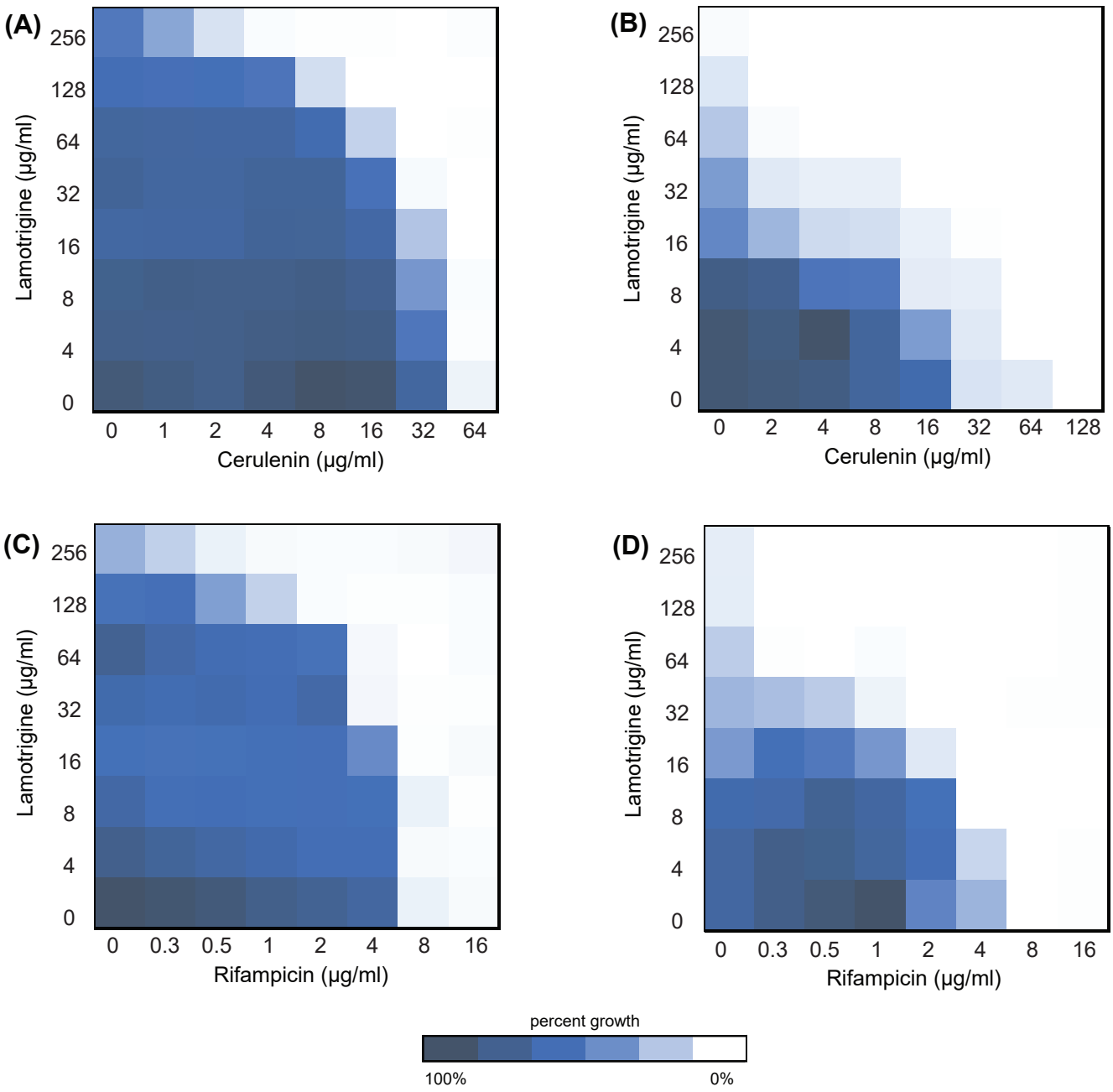

Figure S5. The Synergy of lamotrigine with Antibiotics in Nutrient-Limited and Nutrient-Rich Conditions. Related to Figure 4.

In *E. coli* BW25113 grown in M9 minimal medium (0.4% glucose) at 37°C, lamotrigine was potentiated by the antibiotics **(A)** cerulenin, FICI ≤ 0.5, and **(C)** rifampicin, FICI ≤ 0.5. Both synergistic interactions persisted in nutrient-rich conditions where lamotrigine was also potentiated at 37°C by **(B)** cerulenin, FICI < 0.28, and **(D)** rifampicin, FICI ≤ 0.16.

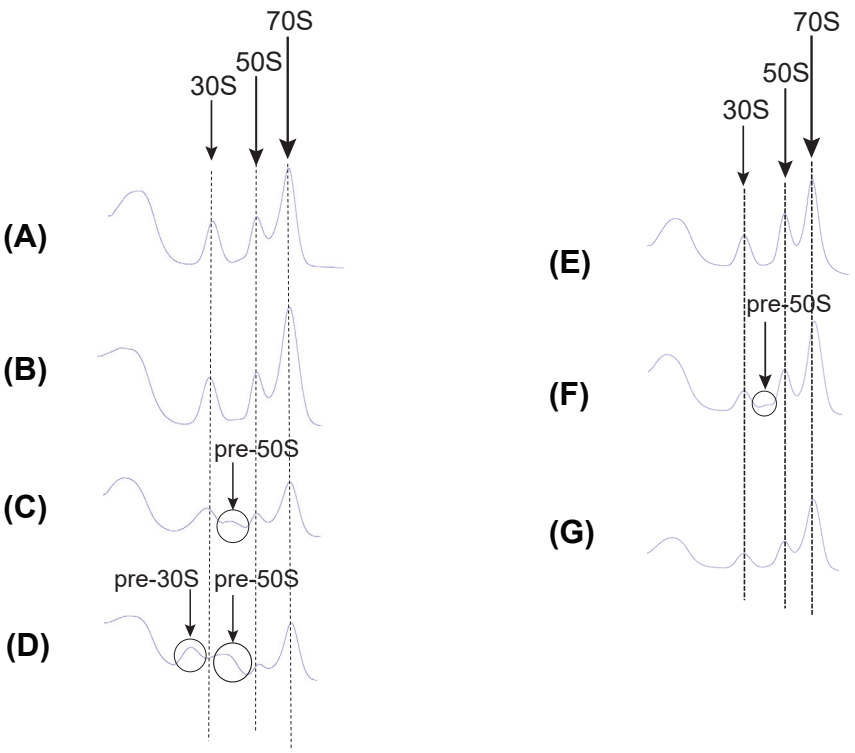

Figure S6. Ribosome Profile Analysis of Lamotrigine and L-norleucine-treated *E. coli* BW25113 at 15°C and 37°C. Related to Figure 4.

E. coli BW25113 at 15°C **(A-D)** and 37°C **(E-G)** in the absence or presence of sub-inhibitory lamotrigine or L-norleucine concentrations. Ribosomal accumulation was monitored using UV absorbance at 260 nm. **(A, E)** Untreated *E. coli* BW25113 cells grown in M9 minimal medium (0.4% glucose) did not accumulate immature pre-30S or pre-50S ribosomal particles. **(B)** Similar results to **(A)** were observed for untreated *E. coli* BW25113 grown in LB medium. **(C)** Lamotrigine-treated *E. coli* BW25113 cells grown in M9 minimal medium (0.4% glucose) accumulated immature pre-50S ribosomal particles. **(D)** Lamotrigine-treated *E. coli* BW25113 cells grown in LB medium resulted in immature pre-30S and pre-50S ribosomal particles. **(F)** Lamotrigine-treated *E. coli* BW25113 cells grown in M9 minimal medium (0.4% glucose) accumulated some immature pre-50S ribosomal particles. **(G)** L-norleucine-treated *E. coli* BW25113 cells grown in M9 minimal medium (0.4% glucose) did not accumulate immature ribosomal particles.

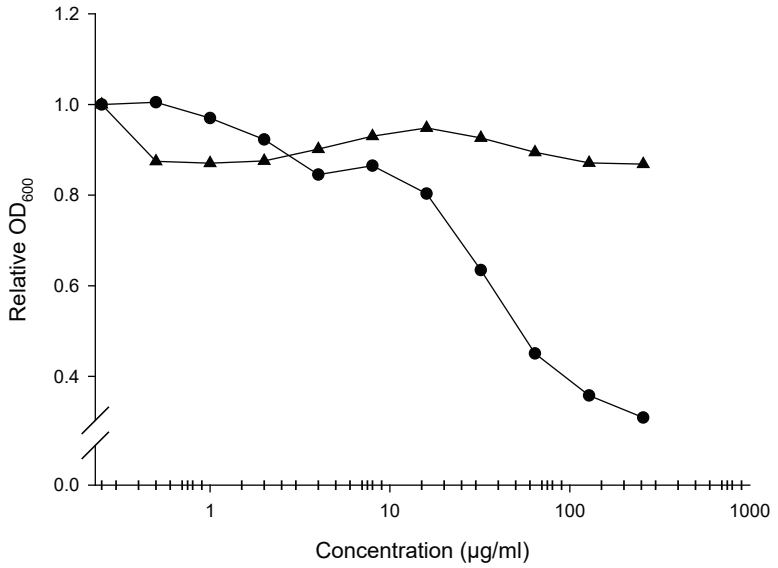

Figure S7. Growth Inhibitory Activity of Thiopurine Analogues in *E. coli* BW25113. Related to Figure 5 and Figure 6.

Potency analysis of 6-mercaptopurine (circles) and 6-thioguanine (triangles) against *E. coli* BW25113 grown in M9 minimal medium (0.4% glucose). The growth inhibitory activity of both nutrient synthesis probes was determined as described in determination of minimal inhibitory concentrations, Transparent Methods.

Transparent Methods

Bacterial Strains and Culture Conditions

All antibiotics and chemicals used in the study were purchased from Sigma Aldrich. The strains used in this study were *E. coli* BW25113, Δ*bioP* (*E. coli* parent strain BW25113, (Baba et al., 2006)), and the *E. coli* IF2 mutant (mutant 1) (*E. coli* parent strain BW25113, (Stokes et al., 2014)). In all experiments, cells were prepared to a final working inoculum of 10^5 CFU/ml. Bacterial cells were grown overnight in M9 minimal medium (0.4% glucose) or LB medium and then diluted 1:50 in fresh M9 minimal medium or LB medium, respectively, and grown at 37°C with aeration at 250 rpm to an OD_{600} of 0.4 (mid-log culture). Cells grown in M9 minimal medium were then diluted 1:1,000 in fresh M9 minimal medium, while those grown in LB medium were diluted 1:10,000 in fresh LB medium, unless stated otherwise.

Determination of Minimal Inhibitory Concentrations

The minimal inhibitory concentration (MIC) for all compounds was determined to inform on the starting concentrations in the checkerboard assays. *E. coli* strains were grown and prepared to a final working inoculum in M9 minimal or LB medium as described above, unless stated otherwise. These cells were then added to a 96-well assay plate containing 2-fold serial dilutions of one of the compounds of interest, where concentrations ranged from 256 μg/ml to 0 μg/ml. Prior to incubation, absorbance at 600 nm (OD_{600}) of the 96-well assay plates was measured using the Tecan plate reader (Infinite M1000). Assay plates were then incubated at 37°C in a stationary incubator for 18 h and OD_{600} was measured. Growth (G) at each exposed concentration was determined as follows

$$G = G_{t=18} - G_{t=0}$$

where $G_{t=18}$ corresponds to the absorbance measured after 18 h of incubation, and $G_{t=0}$ corresponds to the absorbance measured prior to incubation. From here, percent residual growth (%G) was calculated, as follows, to determine the MIC of the compound of interest

$$\%G = \frac{G_i}{G_0}$$

where G_i represents the growth in one of the 12 wells exposed to the different concentrations of the tested compound, and G_0 represents the growth in the well that was not exposed to the tested compound. The concentration that resulted in a percent residual growth ≤ 10% was deemed as the MIC of the tested compound.

Checkerboard Assays

E. coli strains were grown and prepared to a final working inoculum in M9 minimal or LB medium as described above, unless stated otherwise. The checkerboard assays were done as 8 × 8 dose-point matrices. All compounds were prepared as 2-fold serial dilutions starting at 4 × MIC to 0 μg/ml. Absorbance (OD_{600}) was measured prior to and post incubation at 37°C in a stationary incubator. To define interaction of the combination, the fractional inhibitory concentration index (FICI) for each checkerboard assay was calculated as follows

$$FICI = \frac{MIC_{A,X}}{MIC_A} + \frac{MIC_{B,X}}{MIC_B}$$

where $MIC_{A,X}$ is the MIC of compound A in combination with compound B, MIC_A is the MIC of compound A on its own, $MIC_{B,X}$ is the MIC of compound B in combination with compound A, and MIC_B is the MIC of compound B on its own. FICI values ≤ 0.5 were synergistic interactions, values > 2 were antagonistic, and values > 0.5 and ≤ 2 were indifferent (Krogstad et al., 1986). All highlighted interactions were done in biological duplicates. Of note, checkerboard assays

constituting the chemical-chemical interaction matrix were done in the *E. coli* parent strain BW25113, which was grown and prepared to a final working inoculum in M9 minimal medium as described above.

Hierarchical Clustering of the Chemical-Chemical Interaction Profiles

The hierarchical cluster was compiled using the statistical computing and graphics programming language, R. The ward.2 clustering method, which clusters datasets based on the least variance between *n* groups (Murtagh and Legendre, 2014), was implemented in the heatmap.2 function found in the gplots library. The dataset introduced to R comprises the FICIs of all 990 combinations.

Assessment of the Synergy of MAC13772 with Cerulenin in the *E. coli* Mutant Strain Δ*bioP*

The synergy of MAC13772 with cerulenin was assessed in the *E. coli* mutant strain Δ*bioP* (Baba et al., 2006). The Δ*bioP* mutant strain was prepared to a mid-log culture in M9 minimal medium, as described above, to deplete the cells from any extracellularly available biotin. The mid-log culture was then diluted 1:10,000 in fresh LB medium. The MIC of the compounds was determined, and the checkerboard assays were prepared and analyzed as previously described.

Ribosome Profiling by Sucrose Density Gradient Analysis

A single colony of *E. coli* BW25113 was inoculated in 5 ml of M9 minimal medium (0.4% glucose) and grown overnight at 37°C with aeration at 250 rpm. The overnight culture was then diluted 1:20 in 50 ml of fresh M9 minimal medium (0.4% glucose) to obtain an OD600 of ~ 0.05, and grown at 37°C or 15°C with aeration at 250 rpm to an OD600 of 0.2 (early-log). Consequently, the early-log culture was treated with a sub-inhibitory concentration of lamotrigine or L-norleucine, and allowed to grow for 1 h and 16 h at 37°C and 15°C,

respectively, with aeration at 250 rpm. Cells were then harvested by centrifugation (4,000 rpm at 4°C for 30 min), resuspended in 5 ml chilled ribosome buffer (20 mM Tris-HCl, pH 7.0, 10.5 mM MgOAc, 100 mM NH4Cl, and 3 mM β-mercaptoethanol), and lysed using a cell disruptor set at 13 kpsi. Cell lysates were clarified at 24,000 rpm at 4°C for 45 min, and the supernatant was collected and loaded onto 35 ml 10-45% sucrose gradients for ultracentrifugation (18,700 rpm at 4°C for 17 h). The gradients were then analyzed using an AKTA Prime FPLC equipped with a UV flow cell, which was set at an absorbance of 260 nm (Stokes et al., 2014). For each set of treated-cultures, a control culture without treatment was also harvested, lysed, clarified, and analyzed.

Supplemental References

Baba, T., Ara, T., Hasegawa, M., Takai, Y., Okumura, Y., Baba, M., Datsenko, K.A., Tomita, M., Wanner, B.L., and Mori, H. (2006). Construction of *Escherichia coli* K-12 in-frame, single-gene knockout mutants: the Keio collection. Mol Syst Biol *2*, 2006.0008-2006.0008.

Krogstad, D., Moellering, R.J., and Lorian, V. (1986). Antibiotics in laboratory medicine. Baltimore: Williams and Wilkins.

Murtagh, F., and Legendre, P. (2014). Ward's hierarchical agglomerative clustering method: which algorithms implement Ward's criterion? J Classif *31*, 274-295.

Stokes, J.M., Davis, J.H., Mangat, C.S., Williamson, J.R., and Brown, E.D. (2014). Discovery of a small molecule that inhibits bacterial ribosome biogenesis. eLife *3*, e03574.